Electron-phonon interactions in perovskites containing Fe and Cr studied by Raman scattering using oxygen-isotope and cation substitution

Jakob Andreasson,* Joakim Holmlund, Ralf Rauer, Mikael Käll, and Lars Börjesson
Department of Applied Physics, Chalmers University of Technology, Göteborg, Sweden

Christopher S. Knee
Department of Chemistry, Göteborg University, Göteborg, Sweden

Annika K. Eriksson and Sten-G. Eriksson
Department of Environmental Inorganic Chemistry, Chalmers University of Technology, Göteborg, Sweden

Michael Rübhausen
Institut für Angewandte Physik, Universität Hamburg, Hamburg, Germany

Rajit P. Chaudhury
Department of Physics and Texas Center for Superconductivity, University of Houston, Houston, Texas 77204-5002, USA
(Received 31 January 2008; revised manuscript received 18 September 2008; published 3 December 2008)

We use temperature-dependent inelastic light scattering to study the origin of the strong multiphonon scattering of a local oxygen breathing mode present in the mixed *B*-site orthorhombic (space group *Pnma*) perovskite $LaFe_{0.5}Cr_{0.5}O_3$ but absent in isostructural $LaFeO_3$ and $LaCrO_3$. It is seen that the multiphonon scattering is critically sensitive to the presence of both Fe and Cr ions on the *B* site. These results support our interpretation that the multiphonon scattering is activated by local electron-phonon interactions according to the Franck-Condon picture following an Fe-Cr charge transfer. Further, ^{18}O substitution is performed on the $x=0$, 0.04, and 0.5 compounds and clearly shows that all modes appearing above the first-order phonon-scattering region in these compounds originate from higher-order oxygen stretching vibrations. In particular this is the case for the strong second-order scattering dominating the scattering response in $LaFeO_3$. Accordingly we propose that these modes are generated by infrared-active longitudinal optical (IR LO) two-phonon and combination scattering activated by Fröhlich interaction. For $x=0.02$ and 0.04 the characteristic IR LO two-phonon and Franck-Condon multiphonon-scattering profiles mix. We also study the influence of isovalent cation substitution and Sr doping in $AFe_{0.5}Cr_{0.5}O_3$ (A=La, Nd, and Gd) and $La_{1-y}Sr_yFe_{0.5}Cr_{0.5}O_{3-\delta}$ ($y=0$, 0.16, and 0.5) on the strong electron-phonon coupling present in $LaFe_{0.5}Cr_{0.5}O_3$. The Franck-Condon effect in $LaFe_{0.5}Cr_{0.5}O_3$, is not significantly affected by isovalent *A*-site substitution, despite the increasing orthorhombic distortion associated with decreasing *A*-site ionic radii. On the contrary, aliovalent Sr doping causes a rapid decrease in the Franck-Condon scattering. This shows that the strong electron-phonon coupling in these compounds is highly sensitive to local lattice and electronic decoherence but insensitive to global lattice distortions. Finally, a preliminary assignment of the A_g and B_{2g} phonon modes in $AFe_{0.5}Cr_{0.5}O_3$ (A=La, Nd, and Gd) is made based on the present observations and published results for $LaCrO_3$ and $AMnO_3$. The modes associated with oxygen octahedral tilt and bending vibrations are heavily influenced by the magnitude of the orthorhombic distortion.

DOI: 10.1103/PhysRevB.78.235103 PACS number(s): 71.35.Aa, 71.35.Gg

I. INTRODUCTION

The coupling between lattice, charge, and magnetic degrees of freedom in transition-metal (TM) oxides is known to affect the diverse phenomena present in these materials such as high-temperature superconductivity, colossal magnetoresistance (CMR), and half metallicity. In particular, the importance of electron-phonon (el-ph) interactions is exemplified by its role in the CMR effect present in the mixed-valence manganites which has been established both theoretically and experimentally.[1–3]

For the CMR parent compound $LaMnO_3$ it has been proposed that an orbitally mediated el-ph coupling generates strong Raman-active multiphonon scattering characterized by enhanced higher-order phonon scattering according to the Franck-Condon (FC) picture when the incident photon energy is tuned to the Jahn-Teller (JT) gap energy.[4–7] However, despite extensive research the exact assignment of the high-energy modes appearing in many manganites remains a matter of discussion.[8–14] Thus, alternative routes must be explored in order to study the principles of strong el-ph coupling in complex TM oxides and the relation between local and global effects in correlated systems in general.

Using lasers in the visible energy region we have previously shown that an exceptional FC multiphonon effect is present in the mixed *B*-site solid solution $LaFe_{1-x}Cr_xO_3$ ($x=0.1$, 0.5, and 0.9) when the photon energy is within a TM-TM charge-transfer (CT) gap at about 2.4 eV.[15] This multiphonon scattering extends to seven orders at $T=80$ K and, as is expected for FC scattering,[4,5,7] the ratio between

the integrated intensity of first- and second-order scattering is independent of temperature ($I_2/I_1 \approx 0.5$ between $T=300$ and 20 K).[15] Based on our experimental observations and electronic density-of-states calculations[16] we have proposed that the fundamental excitation is a local oxygen breathing mode and that the enhanced Raman scattering is generated by strong orbitally mediated el-ph interactions activated according to the FC picture by a photon induced transfer of an electron from an Fe to an adjacent Cr ion. Such an assignment is also in line with recent observations[17] in other TM oxides. The magnitude of the observed FC scattering in $LaFe_{0.5}Cr_{0.5}O_3$ is to our knowledge unprecedented in complex TM oxides and should prove useful for fundamental studies of the relation between global and local effects in correlated systems in general and el-ph interactions in particular, as well as for the study of transient phenomena.

In the present work we study the way in which the multiphonon scattering, characteristic for the mixed Fe-Cr compounds, emerges from the qualitatively different scattering profiles observed for $LaFeO_3$ (Ref. 15) and $LaCrO_3$.[15,18] Our measurements on the compounds with low and high relative concentrations of Fe and Cr show that characteristic scattering related to el-ph interactions is present between $x=0.02$ and 0.98. This observation supports the Fe to Cr CT model proposed for the activation of the FC mechanism and stresses the importance of local effects in these systems. Further, ^{18}O isotope substitution in $LaFe_{0.5}Cr_{0.5}O_3$ shows that the modes of the multiphonon progression are indeed related to oxygen stretching vibrational excitations. In $LaFeO_3$, isotope substitution shows that the dominating excitations in the second-order scattering region of this compound also have oxygen stretching origin. The absence of Raman-active first-order counterparts of these modes leads us to propose that they are caused by Fröhlich interaction (FI) activated IR LO two-phonon and combination scattering.[19,20] A remarkable similarity of the first- and higher-order scatterings between the results obtained in the Fe-rich $LaFe_{1-x}Cr_xO_3$ compounds ($x=0.02$ and $x=0.04$) using $\lambda=515$ nm ($\hbar\omega=2.41$ eV) and those obtained in $LaFe_{0.5}Cr_{0.5}O_3$ using a UV laser with $\lambda=334$ nm ($\hbar\omega=3.71$ eV) is also observed. This indicates that a FC and IR LO two-phonon resonance mixing can be activated in the mixed Fe-Cr system either by a tuning of the incident photon energy or the chemical composition.

Our results for the low-energy Raman scattering in $LaCrO_3$ are identical with recently reported unpolarized measurements of this compound,[18] including the observation of a orthorhombic (*Pnma*) to rhombohedral ($R\bar{3}c$) structural phase transition (SPT) at about 530 K. However, based on the present results we also assign the strong non-Γ-point mode at about 718 cm^{-1} to the same local breathing vibration that is resonantly enhanced in the mixed *B*-site compounds.

Further, we show that the el-ph coupling in $La_{1-y}Sr_yFe_{0.5}Cr_{0.5}O_{3-\delta}$ is highly sensitive to local changes in the electronic states of the TM ions and local distortions in the lattice caused by the aliovalent Sr doping. On the contrary, isovalent *A*-site substitution (*A*=La, Nd, and Gd) has a limited impact on the FC effect despite the increasing orthorhombic distortion and decrease in O-TM-O bond angles which appear as a consequence of the smaller ionic radii of Nd and Gd.

Finally, we propose a preliminary mode assignment for the main nonresonant Raman-active A_g and B_{2g} phonons in $AFe_{0.5}Cr_{0.5}O_3$, *A*=La, Nd, and Gd. Although it is seen that local *B*-site ordering influences the phonon spectra, the assignment of the modes is made according to the *Pnma* setting of the space group D_{2h}^{16}. This assignment is done in comparison with established results for $LaCrO_3$ (Ref. 18) and $AMnO_3$.[21–23] In particular, increasing orthorhombic distortion causes a significant hardening of the modes related to oxygen octahedral tilt and bending vibrations, similar to what has been observed in $AMnO_3$. We also propose that the sidebands which appear close to the higher-order peaks in the FC scattering in $LaFe_{0.5}Cr_{0.5}O_3$ are combination bands involving the local oxygen breathing mode.

II. EXPERIMENTAL

All samples, $LaFe_{1-x}Cr_xO_3$ ($x=0$, 0.02, 0.04, 0.06, 0.08, 0.10, 0.5, 0.90, 0.92, 0.94, 0.96, 0.98, and 1.0), $AFe_{0.5}Cr_{0.5}O_3$ (*A*=La, Nd, and Gd), and $La_{1-y}Sr_yFe_{0.5}Cr_{0.5}O_{3-\delta}$ ($y=0$, 0.16, and 0.5) were made by solid-state sintering with phase purity confirmed by powder x-ray diffraction. The structural and magnetic properties of $LaFe_{0.5}Cr_{0.5}O_3$ have been extensively studied[24] and the isostructural properties of the other compounds were established at room temperature (RT) using x-ray diffraction. At RT, all samples adopt a pseudocubic structure of orthorhombic symmetry described by the D_{2h}^{16} space group (*Pnma* or *Pbnm* setting). $LaCrO_3$ experiences a SPT at 528 K with a rhombohedral $R\bar{3}c$ high-temperature phase.[18] The $x=0$, 0.5, and 1 compounds are known to have *G*-type antiferromagnetic (AFM) phases below $T_N=750$, 265, and 280 K, respectively. The presence of a weak uncompensated magnetic moment below T_N in $LaFe_{0.5}Cr_{0.5}O_3$ (Ref. 24) indicates a presence of local *B*-site ordering concomitant with the monoclinic $P2_1/n$ space group.

The increasing orthorhombic distortion of $AFe_{0.5}Cr_{0.5}O_3$ (*A*=La, Nd, and Gd) is manifested by a decrease in B-O(2)-B bond angles from 158.6(2)° for *A*=La, to 151(1)° for *A*=Nd, and to 148(1)° for *A*=Gd, as determined from Rietveld analysis of neutron (*A*=La) and x-ray (*A*=Nd and Gd) diffraction data. The ionic radii of La, Nd, Gd, and Sr (in eightfold coordination) are $r_{La}=1.16$ Å, $r_{Nd}=1.109$ Å, $r_{Gd}=1.053$ Å, and $r_{Sr}=1.26$ Å and the atomic masses are $m_{La}=138.91$ a.u., $m_{Nd}=144.24$ a.u., $m_{Gd}=157.25$ a.u., and $m_{Sr}=87.62$ a.u.

All presented spectra using the $\lambda=515$ nm laser line (photon energy $\hbar\omega=2.41$ eV) were recorded using a DILOR-XY800 spectrometer with a microscope setup and a 40× magnification glass-compensating objective generating a spot size of approximately 2 μm in diameter. In this setting the beam power was kept below 1 mW on the sample. This small spot size likely causes local heating in the irradiated spot, in particular at low temperatures and the given temperature readings should be considered as approximate. However, during the course of these measurements several different settings of several different spectrometers were

used showing that the present results are representative over a wide range of irradiation densities.

A double subtractive spectrometer mode was used for the measurements close to the laser line, while a single grating mode and a notch filter was used for the spectra with large Raman shift. The measurements using the UV $\lambda=334$ nm (3.71 eV) laser line was carried out on a custom designed UT3 Raman spectrometer (McPherson) (Ref. 25) with a spot size diameter of less than 20 μm and a beam power at the sample below 10 mW covering an array of randomly oriented single crystallites.

For the $x \geq 0.9$ compounds the grain sizes were too small for measurements on individual crystallites, also with the microsetup, and the measurements were done on randomly oriented crystallite arrays. For all other compounds, the grain sizes were sufficient for measurements on individual crystallites and the measurements were made on selected surfaces representing as-grown crystallographic ac planes due to the strong B-O(2) bonds,[15,18] with the incident direction along the b axis (back scattering configuration). The relative polarizations of incident and scattered light in the presented measurements were mostly parallel (p) activating nonresonant Γ-point modes of A_g and B_{2g} symmetry. For the polarization-dependent measurements on $LaFe_{0.5}Cr_{0.5}O_3$ the sample was oriented with respect to the straight edges representing B-O(2) directions in selected crystallites. For the scattering configurations labeled $x'x'(z'z')$ and $x'z'(z'x')$ the polarization directions of the incoming and scattered light were aligned along the crystallite edges and for the $xx(zz)$ and $xz(zx)$ measurements the sample was rotated by 45°.[15,18]

For the measurements above and below RT the samples were mounted in a Linkam heat cell and a CryoVac cold finger microcryostat, respectively. The scattered signals were recorded using a liquid-nitrogen cooled multichannel charge coupled device (CCD) camera. All spectra presented have been compensated for the thermal Bose-Einstein factor and are shown with vertical offsets for clarity.

For the ^{18}O isotope substitution two similar samples of each compound were treated simultaneously in identical gas flow circuits, one in ^{18}O and one in ^{16}O.[14] The samples treated in ^{16}O were used as references together with untreated samples of each compound.

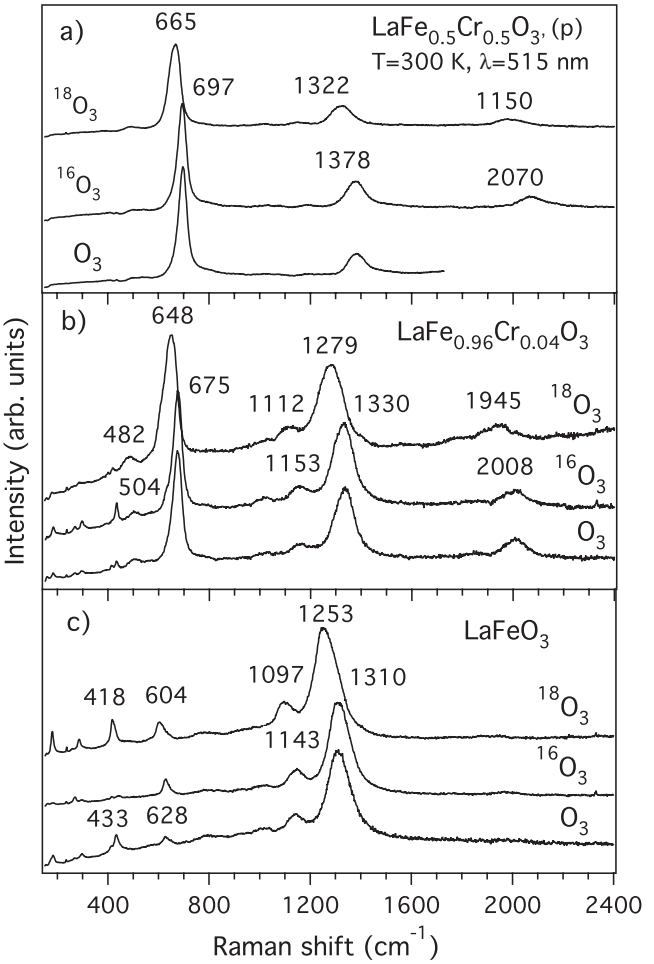

FIG. 1. Effects of oxygen-isotope substitution in: (a) $LaFe_{0.5}Cr_{0.5}O_3$, (b) $LaFe_{0.96}Cr_{0.04}O_3$, and (c) $LaFeO_3$ measured at 300 K using $\lambda=515$ nm and parallel scattering configuration. The spectra labeled $^{18}O_3$ and $^{16}O_3$ are from compounds which have been subjected to identical heating processes in ^{18}O and ^{16}O gas, respectively. The spectra labeled O_3 are from untreated reference samples.

III. RESULTS AND DISCUSSION

This section is organized in the following way: in Sec. III A we present the effects of ^{18}O isotope substitution in $LaFe_{0.5}Cr_{0.5}O_3$, $LaFeO_3$, and $LaFe_{0.96}Cr_{0.04}O_3$. In Sec. III B the nature of the scattering from compounds with high Fe concentration is discussed. Special attention is given to the compositions $LaFeO_3$ and $LaFe_{0.96}Cr_{0.04}O_3$, which are studied over wide temperature ranges. In Sec. III C, the nature of the scattering from compounds with high Cr concentrations is discussed with special attention on $LaCrO_3$. Section III D deals with the effects of isovalent A-site substitution in $AFe_{0.5}Cr_{0.5}O_3$ while Sec. III E covers Sr doping in $La_{1-y}Sr_yFe_{0.5}Cr_{0.5}O_3$. Finally, Sec. III F gives a preliminary mode assignment of the Raman-active modes with A_g and B_{2g} symmetry according to the *Pnma* setting. In this section the detailed nature of the first- and higher-order sidebands in $LaFe_{0.5}Cr_{0.5}O_3$ is also discussed.

A. ^{18}O substitution

Initially we discuss the results obtained by O^{18} isotope substitution in the compounds $LaFe_{0.5}Cr_{0.5}O_3$, $LaFeO_3$, and $LaFe_{0.96}Cr_{0.04}O_3$ (Fig. 1). Here the intention is to identify the origin of the dominating Raman-active modes in the different characteristic scattering profiles.

In $LaFe_{0.5}Cr_{0.5}O_3$ [Fig. 1(a)] it is seen that all of the modes in the FC multiphonon scattering shift to lower energies with O^{18} substitution in line with expectations for FC scattering originating from a local oxygen breathing mode.

The origin of the strong modes present between 1100 and 1400 cm^{-1} in $LaFeO_3$ [Fig. 1(c)] (1153 and 1310 cm^{-1} in LaFe $^{16}O_3$ and 1112 and 1279 cm^{-1} in LaFe $^{18}O_3$) has been briefly addressed in a previous publication where the possibility of a magnetic origin of these modes was also

discussed.[15] Here we show that a significant downshift affects these modes with O^{18} substitution [Fig. 1(c)]. This observation strongly indicates a pure oxygen stretching vibrational origin of the second-order modes in $LaFeO_3$.

Finally, for low Cr substitution levels, the two characteristic scattering-profiles discussed above mix showing a very strong second-order excitation as well as considerable third order scattering [Fig. 1(b)]. In $LaFe_{0.96}Cr_{0.04}O_3$ ^{18}O substitution shows that a downshift of the dominant modes in the first- and higher-order scattering regions occurs also for this compound. As for the compounds above this indicates that these modes originate from pure oxygen stretching vibrations.

The expected shift for an oxygen stretching vibration according to a harmonic-oscillator approximation is about 6% at full substitution.[14] The shifts discussed here are all about 4% corresponding to isotope substitution levels of about 66%. These substitution levels are also in line with measured increases in the masses of the ^{18}O treated samples. Further, we observe that the modes affected by downshifts also broaden with the isotope substitution due to the presence of both ^{16}O and ^{18}O isotopes in the lattice.

We note that although we used parallel scattering configuration for all measurements in the isotope substitution study, some differences in scattering intensities of the low-energy Γ-point modes are seen (e.g., the mode at 433 cm^{-1} in $LaFeO_3$ and 418 cm^{-1} in $LaFe^{18}O_3$ is very weak in $LaFe^{16}O_3$). This reflects different sample orientations affecting the scattering of the specific first-order Raman-active modes by the influence of the symmetry selection rules. However, the high-energy modes are not affected indicating that they are related to local excitations which are not subject to general symmetry selection rules.

B. High Fe concentration

In order to study the emergence of the el-ph interaction in $LaFe_{1-x}Cr_xO_3$ and to assign the excitations in the second-order energy region of $LaFeO_3$, a series of samples with low Cr content ($x \leq 0.10$) were studied at 300 K (Fig. 2).

A more detailed discussion about the nature of the Raman-active Γ-point modes in the mixed Fe-Cr compounds, $LaCrO_3$ and $LaFeO_3$ is provided elsewhere (Sec. III F and Ref. 18) and here only a simplified group assignment for $LaFe_{1-x}Cr_xO_3$ is presented (Fig. 2). Modes caused by La vibrations are present below 200 cm^{-1} (labeled *A*), modes between 200 and 300 cm^{-1} are oxygen octahedral tilt modes (*T*), modes between 400 and 450 cm^{-1} are oxygen octahedral bending vibrations (*B*) and modes above 500 cm^{-1} are oxygen stretching vibrations (*S*).[21–23,26,27] With decreasing Cr concentration the low-energy spectra of the Fe-rich compounds show a continuous evolution into the scattering response of $LaFeO_3$.

The greatest change in the first-order spectrum is seen in the region dominated by the local oxygen breathing mode at about 700 cm^{-1} which is resonantly enhanced in the mixed *B*-site compounds. This mode shows a continuous decrease in intensity between $x=0.10$ and $x=0.02$ and then completely disappears in $LaFeO_3$ (Fig. 2). This is a strong indication that

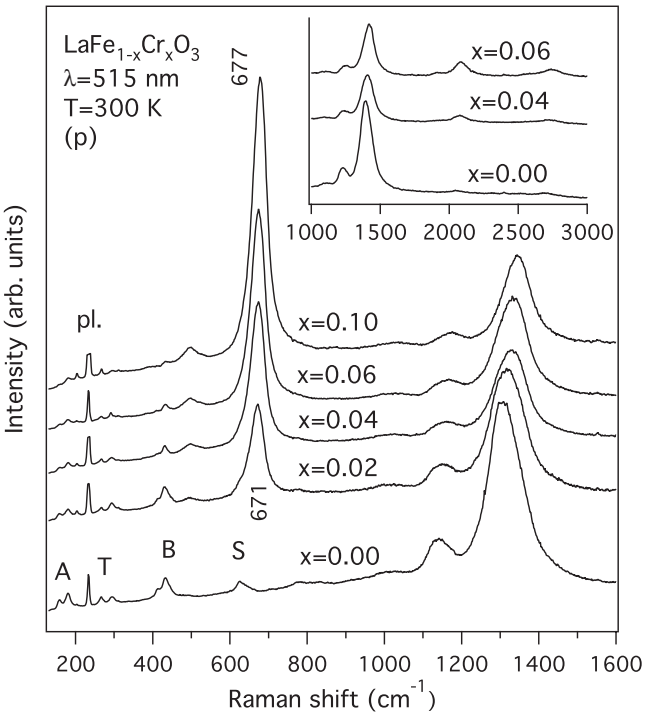

FIG. 2. First- and higher-order Raman spectra of the $LaFe_{1-x}Cr_xO_3$ compounds with low Cr contents, $x=0.00$, 0.02, 0.04, 0.06, and 0.10 measured at 300 K using $\lambda=515$ nm. The spike labeled pl. is a known plasma line of the setup at 236 cm^{-1}. Inset: the characteristic FC resonance with a series of higher-order excitations is clearly present for $x \geq 0.06$, below which the third- and higher-order decrease continuously.

the mechanism behind the resonant enhancement of the oxygen breathing mode depends critically on the presence of both Fe and Cr ions on the *B* site. Further, the fact that the FC multiphonon scattering remains also for quite low Cr concentrations (Fig. 2 and inset) shows that it appears as an effect of a local el-ph interaction.

In the compounds with low Cr concentration the second-order features in the 1100–1400 cm^{-1} energy region appear to be only partly caused by the second order of the oxygen breathing mode. As Cr content decreases the dominant high-energy feature increases in intensity, although the first-order breathing mode decreases significantly between $x=0.10$ and $x=0.02$ and disappears completely for $x=0$ (Fig. 2). Thus, as Cr concentration decreases the FC scattering yields to a different effect characterized by dominant second-order scattering with no Raman-active first-order scattering and only very weak third-order scattering. It is also seen that the dominant second-order mode shifts to lower energies with decreasing Cr content (Fig. 2).

From the results of the ^{18}O substitution we have established that the second-order modes in $LaFeO_3$ are of oxygen vibrational origin. However, the absence of first-order modes with suitable energies indicates that they are not generated by two-phonon scattering of Raman-active phonons. Instead we recall that strong IR LO phonon bands have been reported in $LaFeO_3$ at energies around 488 and 630 cm^{-1}.[28] Although the reported energy of the highest IR LO phonon (630 cm^{-1}) is slightly lower than half of the energy of the

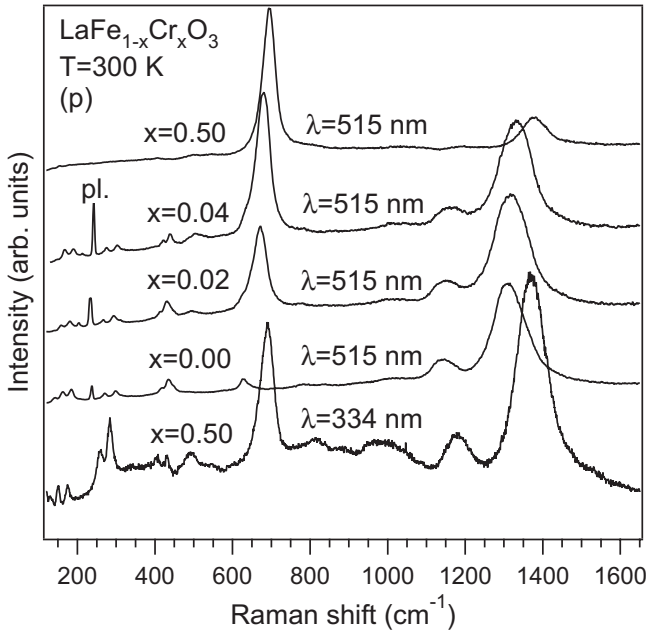

FIG. 3. The first- and second-order scattering from the Fe-rich compounds ($x=0.02$ and $x=0.04$) using $\lambda=515$ nm and that from $LaFe_{0.5}Cr_{0.5}O_3$ using UV $\lambda=334$ nm show remarkable similarities. The spectra are normalized for comparison and do not show correct absolute scattering intensities.

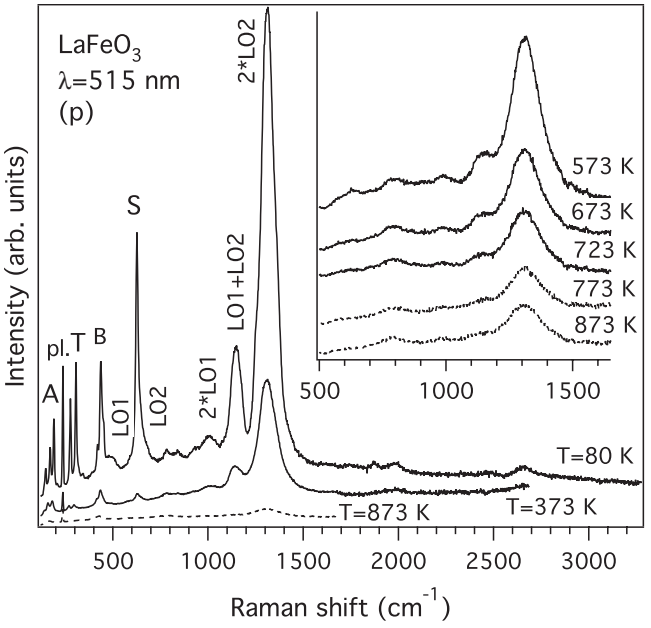

FIG. 4. Temperature-dependent Raman spectra of $LaFeO_3$. Solid lines are spectra measured below the AFM ordering temperature $T_N=750$ K. Inset shows the high-energy scattering across the AFM ordering temperature $T_N=750$ K. The high-energy scattering is prominent also above 750 K and no saturation is seen below T_N.

1310 cm^{-1} peak observed here (Fig. 2), we propose that the 1310 cm^{-1} peak is caused by Fröhlich interaction activated two-phonon scattering of the 630 cm^{-1} IR LO mode and that the 1143 cm^{-1} peak (Fig. 2) is caused by a combination scattering of the 630 and 488 cm^{-1} IR LO bands. This assignment is further supported by low-temperature measurements of $LaFeO_3$ and $LaFe_{0.96}Cr_{0.04}O_3$ discussed below.

In the compounds with low Cr content, in particular for $x=0.02$ and 0.04, the two different second-order scattering mechanisms coexist and their characteristic first- and higher-order Raman spectra mix. Interestingly, the results from these compounds using the visible laser $\lambda=515$ nm (Figs. 2 and 3) are quite similar to those obtained using a UV incident photon energy at 3.71 eV ($\lambda=334$ nm) on $LaFe_{0.5}Cr_{0.5}O_3$ (Fig. 3). This observation indicates that a coexistence between FC multiphonon and IR LO two-phonon scattering in $LaFe_{1-x}Cr_xO_3$ can be achieved either by resonance mixing or chemical tuning. A possible mechanism for the IR LO two-phonon activation can be a O-TM CT. Further resonance studies combined with detailed electronic band-structure calculations could verify this.

1. *Temperature dependence in* $LaFeO_3$

Temperature-dependent measurements of $LaFeO_3$ between 80 and 893 K reveal a continuous decrease in definition and complexity of the first-order phonon spectrum with increasing temperature (Fig. 4). At room temperature the main characteristic *Pnma* Γ-point modes (*A*, *T*, *B*, and *S*) are still visible but at 893 K only the bending mode at about 400 cm^{-1} remains (Fig. 4). This indicates that the compound moves toward a structure with higher symmetry above RT. However, no discontinuous structural phase transition (SPT) was observed. In addition to the Raman-active Γ-point phonons two broad modes are observed, at low temperatures, at about 500 and 650 cm^{-1} labeled LO1 and LO2, respectively (Fig. 4). The LO2 mode is underlying the sharp stretching mode (*S*) at about 650 cm^{-1}. We assign these modes to the IR LO phonon bands reported at about these energies.[28]

In the second-order scattering region a third mode at about 1000 cm^{-1} appears at low temperatures in addition to the two modes seen already at 300 K (Fig. 4). Comparing the energies of the two proposed IR LO phonon modes and these three peaks we propose that the mode at about 1000 cm^{-1} is a two phonon of the 500 cm^{-1} IR LO mode (2^*LO1), the mode at about 1310 cm^{-1} is a two phonon of the 650 cm^{-1} IR LO mode (2^*LO2), and the mode at about 1140 cm^{-1} is a combination band of the 500 and 650 cm^{-1} IR LO modes (LO1+LO2) (Fig. 4).[19,20]

Finally, we note that the modes between 1100 and 1300 cm^{-1} show no signs of saturation below $T_N=750$ K (Fig. 4, inset). This is another indication that these modes are not related to two-magnon scattering.

2. *Temperature dependence in* $LaFe_{0.96}Cr_{0.04}O_3$

In the preceding sections we have established four basic features of the $LaFe_xCr_{x-1}O_3$ system (III A, III B, and III B 1). First, ^{18}O isotope substitution shows that all modes present in the higher-order scattering regions are related to oxygen stretching vibrations (III A). Second, for substitution levels $x \geq 0.02$ a FC progression of the oxygen breathing mode influences the first- and higher-order scattering (III B). Third, in $LaFeO_3$ strong second-order modes are activated by

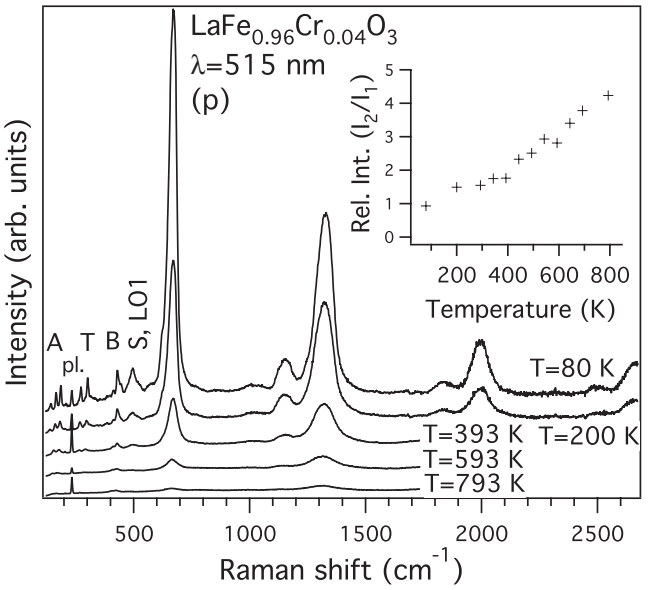

FIG. 5. Temperature-dependent Raman spectra of $LaFe_{0.96}Cr_{0.04}O_3$. Inset shows the temperature dependence of the relative intensities of the dominant first (I_1) and second (I_2) order features located at about 675 and 1310 cm^{-1}, respectively.

IR LO two-phonon scattering (III B and III B 1) and combination scattering. Fourth, for low substitution levels ($x=0.02$ and 0.04) these two characteristic higher-order scattering profiles mix (III B).

To further study the complex situation in the Fe-rich compounds we performed temperature-dependent measurements on $LaFe_{0.96}Cr_{0.04}O_3$ between 793 and 80 K (Fig. 5). As in $LaFeO_3$ the main Raman-active *Pnma* Γ-point modes appear in the characteristic *A*, *T*, *B*, and *S* regions and we see a continuous decrease in definition of the first-order vibrational spectrum with increasing temperature (Fig. 5) but no discontinuous SPT.

More interestingly, fitting the dominant first and second-order peaks around 675 and 1310 cm^{-1} with one Lorentzian profile each it is seen that their relative integrated intensity I_2/I_1 increases substantially with temperature (Fig. 5, inset). This behavior is particularly clear at temperatures above RT but remains also at low temperatures and is in contrast to what has been seen for pure FC scattering in $LaFe_{0.5}Cr_{0.5}O_3$ where the ratio between the first- and second-order peaks of the FC progression is independent of temperature between 300 and 20 K.[15] This result indicates that an additional scattering process is influencing the scattering in the second-order region and the present temperature behavior of the second-order scattering is similar to that observed for IR LO two-phonon modes in other TM oxides.[19,29] We also note that the apparent decrease in the slope of I_2/I_1 (Fig. 5, inset) below about 400 K may be caused by local heating in the irradiated spot which is likely to have an increasing influence with decreasing temperature.

A closer inspection of the low-temperature measurements of $LaFe_{0.96}Cr_{0.04}O_3$ can provide a detailed assignment of the three second-order features at 1000, 1140, and 1350 cm^{-1} (Fig. 6). This assignment is similar to that provided earlier for $LaFeO_3$ but also includes a considerable contribution

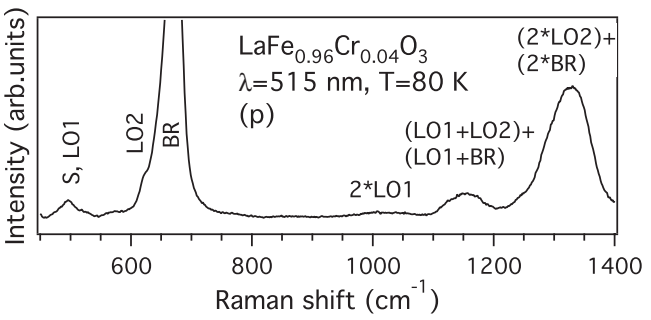

FIG. 6. The second-order scattering in $LaFe_{0.96}Cr_{0.04}O_3$ at $T=80$ K is constructed from two-phonon and combination scattering of the two IR LO modes (LO1 and LO2) and the local oxygen breathing mode.

from the first- and second-orders of the local oxygen breathing mode (BR). In addition to the strong peak at about 670 cm^{-1} which is dominated by the local breathing mode, two weaker features at about 630 cm^{-1} (LO2) and 500 cm^{-1} (LO1) can be identified in correspondence with the situation in $LaFeO_3$ (the broad LO1 feature is underlying a sharper Raman-active Γ-point oxygen stretching mode and the LO2 mode is seen as a low-energy shoulder of the breathing mode) (Fig. 6). Combining these modes the second-order scattering profile can be constructed as a superposition of second-order FC scattering of the breathing mode, IR LO two-phonon scattering, and combination bands (Fig. 6). At energies above the second-order region the FC scattering of the local breathing mode generates third- and higher-order scattering (Fig. 5).

C. High Cr concentration

The first-order Raman-active Γ-point phonons (below about 600 cm^{-1}) of the low-temperature orthorhombic and high-temperature rhombohedral phases of $LaCrO_3$ have been studied in detail and assigned to specific vibrational modes according to their symmetry properties and lattice-dynamical calculations by Iliev *et al.*[18] The present measurements were performed on arrays of randomly oriented microcrystallites and our results for the first-order region of $LaCrO_3$ are practically identical to those reported for unpolarized measurements in Ref. 18. Again the main Raman-active *Pnma* Γ-point modes appear mainly in the characteristic *A*, *T*, *B*, and *S* regions. Further, we see that for Cr concentrations above $x=0.90$ in $LaFe_{1-x}Cr_xO_3$ the nonresonant low-energy modes evolve continuously into the characteristic $LaCrO_3$ spectrum (Fig. 7).

At $T=300$ K, all Cr rich compounds $x \geq 0.90$ except $LaCrO_3$ show the characteristic FC scattering of the local oxygen breathing mode at about 700 cm^{-1}. In $LaCrO_3$ broad features are seen in the first- and second-order regions but no third-order scattering is observed (Fig. 7). This again highlights the necessity of the presence of both Fe and Cr in the structure for the activation of the FC scattering and the local nature of the el-ph interaction

It was previously observed by Iliev *et al.*[18] that the 700 cm^{-1} energy region in $LaCrO_3$ hosts two peaks with

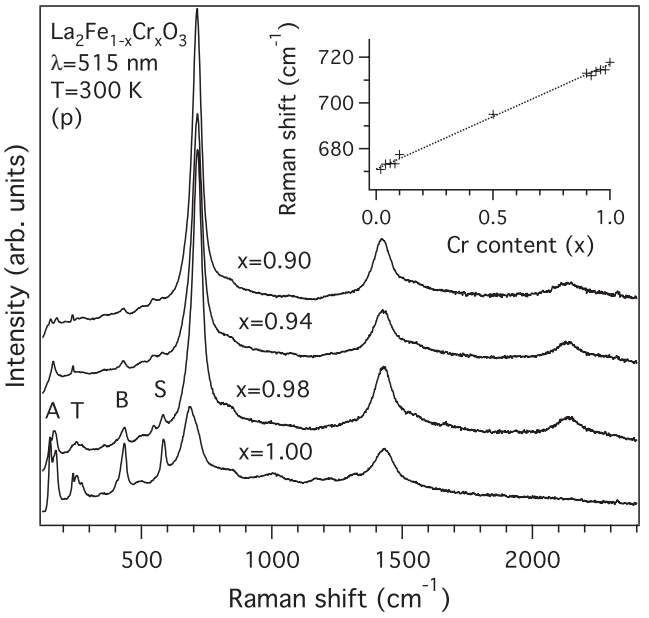

FIG. 7. First- to third-order Raman spectra of the $LaFe_{1-x}Cr_xO_3$ compounds with high Cr content (x=0.90, 0.94, 0.98, and 1.00). The characteristic FC resonance is clearly present for $x \leq 0.98$. Only the fully substituted compound $LaCrO_3$ displays a qualitatively different scattering response with strong second-order scattering but no third- or higher-order modes at T=300 K. Inset shows the linear shift of the local breathing mode over the x=0.02 to x=1 substitution interval. The straight line is a guide to the eyes.

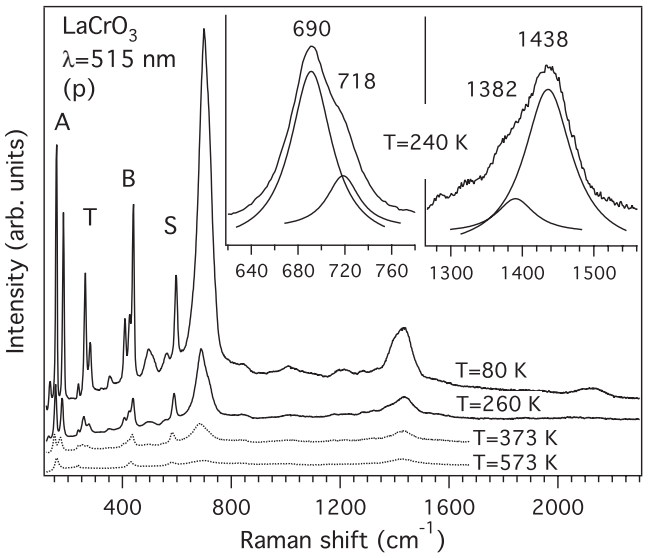

FIG. 8. Temperature-dependent Raman spectra of $LaCrO_3$ measured using λ=515 nm. Solid lines indicate measurements below the AFM ordering temperature T_N=280 K. Inset: below $T \approx 240$ K the broad second-order feature can be resolved into two modes located at 1382 and 1438 cm^{-1}. These correspond to two-phonon scattering of the local oxygen vibrations at 690 and 718 cm^{-1}. The four main peaks seen in the inset are fitted with Lorentzian profiles.

A_g-like symmetry properties at about 690 and 718 cm^{-1}. Furthermore, they show that the intensities of these modes decrease significantly upon annealing in vacuum and it is argued that they cannot be assigned to Γ-point phonons or phonon density-of-states scattering. Instead it is proposed that the unannealed compound has an oxygen excess and cation deficiency and that charge neutrality is retained by part of the chromium being Cr^{4+} (d^2) instead of Cr^{3+} (d^3). Under these circumstances local distortions appear in the oxygen lattice around these sites according to the anisotropic orbital configuration of the partially filled t_{2g} levels and local el-ph interactions can be expected. The authors also mention that a similar A_g-like mode in $La_{1-x}Sr_xMn_{1-y}Cr_yO_3$ has recently been assigned to a local breathing mode.[17] We note from our present data that the resonant local breathing mode in $LaFe_{1-x}Cr_xO_3$ shifts linearly to higher frequencies with increasing Cr content (Fig. 7, inset). At RT it is located at about 671 cm^{-1} for x=0.02 and shifts to 677 cm^{-1} for x=0.10, 695 cm^{-1} for x=0.5, 713 cm^{-1} for x=0.90, and 715 cm^{-1} for x=0.98. According to this sequence we propose that the 718 cm^{-1} mode in $LaCrO_3$ (Fig. 8) is caused by a local oxygen breathing mode of the same character as that which is resonantly enhanced by the FC process in the mixed B-site compounds.

1. Temperature dependence in $LaCrO_3$

In order to further study the first and higher order scattering in $LaCrO_3$ we performed temperature-dependent measurements between 80 and 573 K covering the first to third order energy regions (Fig. 8). The evolution of the first-order scattering follows that reported in Ref. 18 including the observation of the SPT at about 530 K between the low-temperature orthorhombic ($Pnma$) and high-temperature rhombohedral ($R\bar{3}c$) phases.

At low temperatures the feature around 1400 cm^{-1} obtains a clear double peak structure and the two peaks at about 1382 and 1438 cm^{-1} correspond to second-order scattering of the 690 and 718 cm^{-1} modes discussed above (Fig. 8, inset). Comparing the relative intensities of the first- and second-order scattering of the 690 and 718 cm^{-1} modes we see that although the breathing mode at 718 cm^{-1} has lower intensity than the 690 cm^{-1} mode the second-order scattering is dominated by the two-phonon breathing mode which is present up to 573 K while the second order of the 690 cm^{-1} mode appears below RT. Further, third-order scattering appears below 200 K (Fig. 8), but due to the weakness and broad nature of this excitation we cannot determine if this mode is caused by third-order scattering of the 690 cm^{-1} or the 718 cm^{-1} mode or if both contribute. However, given the large drop in intensity between the one- and two-phonon scattering of the 690 cm^{-1} mode it is likely that the broad low-temperature third-order feature originates from the local breathing mode. The complex behavior of the first- and higher-order non-Γ-point oxygen modes indicates a temperature-dependent interplay between structural and electronic properties in $LaCrO_3$ and should be studied in greater detail in order to gain further insight into the interaction between different el-ph interaction mechanisms.

Below RT a broad mode appears at about 500 cm^{-1} the origin of which is at present unclear.[18] However, we note that the weak second-order features observed at about 1000 and

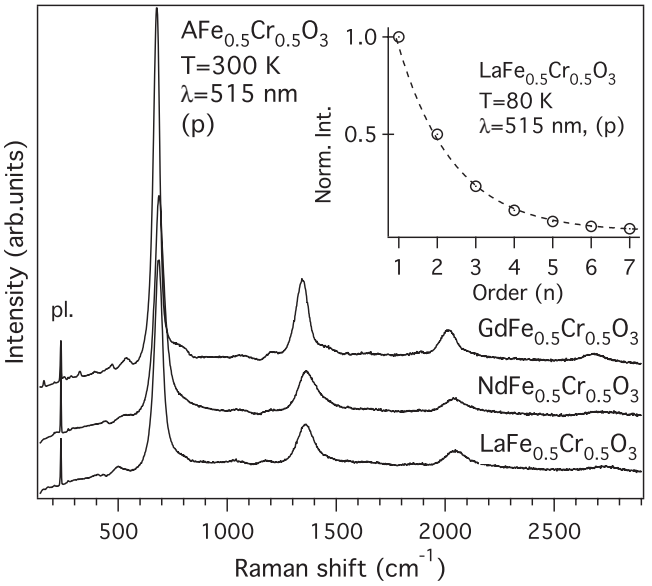

FIG. 9. The first- and higher-order spectra of the mixed *B*-site compounds $A\mathrm{Fe}_{0.5}\mathrm{Cr}_{0.5}\mathrm{O}_3$, *A*=La, Gd, and Nd measured at $T=300$ K using $\lambda=515$ nm and parallel polarization. Inset: the FC scattering present in $\mathrm{LaFe}_{0.5}\mathrm{Cr}_{0.5}\mathrm{O}_3$ for $\hbar\omega=2.41$ eV follows $I_n \propto 0.5^n$ (dashed line shows $2^*0.5^n$).

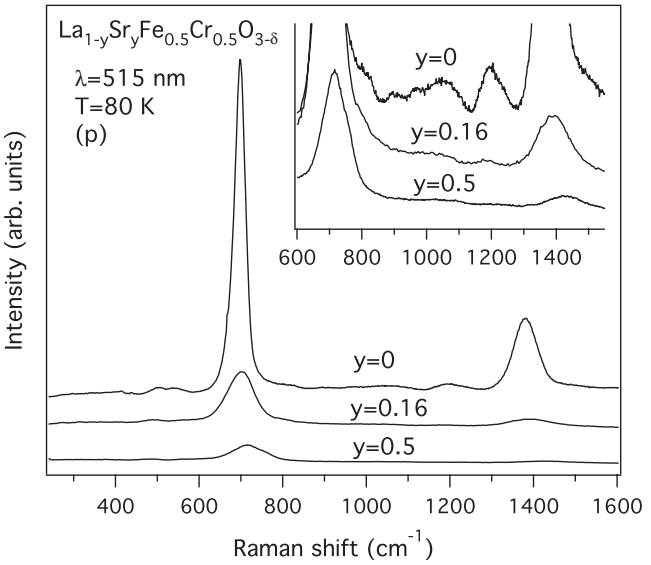

FIG. 10. First- and second-order spectra of the Sr doped compounds $\mathrm{La}_{1-y}\mathrm{Sr}_y\mathrm{Fe}_{0.5}\mathrm{Cr}_{0.5}\mathrm{O}_{3-\delta}$ ($y=0$, 0.16, and 0.50) measured at $T=80$ K using $\lambda=515$ nm and parallel polarization. Inset: although strongly reduced, the second-order scattering remains also for $y=0.16$ and 0.5.

1200 cm^{-1} at 80 K (Fig. 8) may be caused by two-phonon scattering of this mode and combination scattering of the 500 and 700 cm^{-1} features, respectively.

Finally, we comment that although the temperature study of LaCrO_3 (Fig. 8) covers the AFM ordering temperature ($T_N=280$ K) no magnetic scattering is observed.

D. Isovalent *A*-site substitution

Isovalent *A*-site substitution has been extensively used to clarify the detailed nature of the oxygen vibrations in the manganites AMnO_3. As is the case for the manganites, $\mathrm{LaFe}_{0.5}\mathrm{Cr}_{0.5}\mathrm{O}_3$, $\mathrm{NdFe}_{0.5}\mathrm{Cr}_{0.5}\mathrm{O}_3$, and $\mathrm{GdFe}_{0.5}\mathrm{Cr}_{0.5}\mathrm{O}_3$ belong to the same orthorhombic D_{2h}^{16} space group but are subject to increasing orthorhombic distortions and decreasing unit-cell volume as the *A*-site ion radius decreases.

The impact of isovalent *A*-site substitution in $A\mathrm{Fe}_{0.5}\mathrm{Cr}_{0.5}\mathrm{O}_3$ on the first- and higher-order scattering is shown in Fig. 9. It is seen that the first- and higher-order scattering in $\mathrm{NdFe}_{0.5}\mathrm{Cr}_{0.5}\mathrm{O}_3$ and $\mathrm{GdFe}_{0.5}\mathrm{Cr}_{0.5}\mathrm{O}_3$ is qualitatively similar to that of $\mathrm{LaFe}_{0.5}\mathrm{Cr}_{0.5}\mathrm{O}_3$ where the integrated intensities of the first- and higher-order (n) of the local breathing mode follows $I_n \propto 0.5^n$ (Fig. 9, inset) as expected for FC scattering.[6] The fact that the increasing orthorhombic distortion does not significantly affect the FC scattering of the local oxygen breathing mode at about 700 cm^{-1} shows that the activation of the strong el-ph coupling is insensitive to global structural distortions as long as the local electronic environment of the FC active sites remains unperturbed.

E. Aliovalent *A*-site substitution

Contrary to the limited effects of isovalent *A*-site substitution, introduction of Sr on the *A*-site strongly influences the scattering already at low substitution levels. In $\mathrm{La}_{1-y}\mathrm{Sr}_y\mathrm{Fe}_{0.5}\mathrm{Cr}_{0.5}\mathrm{O}_{3-\delta}$ three separate effects of the Sr substitution are observed: (1) A decrease in absolute scattering intensity of all first- and higher-order Raman-active modes (Figs. 10 and 11). (2) A loss of definition seen primarily for the low-energy first-order modes (Fig. 11). (3) A significant decrease in the relative intensity between the second and first order of the local oxygen breathing mode I_2/I_1 (Fig. 10). This decrease is quite substantial from about 0.5 for $x=0$ to less than 0.2 for $x=0.16$.

Of these three observations the first two may be associated with non-FC related effects. The general decrease in absolute scattering intensities of nonresonant phonon modes may be related to changes in the optical properties such as penetration depth and absorption. An observed color change of the samples from red (for $x=0$) to dark brown or black

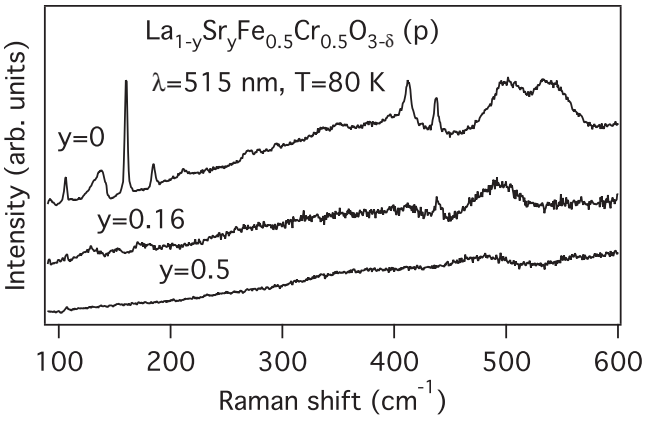

FIG. 11. Low-energy region of $\mathrm{La}_{1-y}\mathrm{Sr}_y\mathrm{Fe}_{0.5}\mathrm{Cr}_{0.5}\mathrm{O}_{3-\delta}$ ($y=0$, 0.16, and 0.5) measured at $T=80$ K using $\lambda=515$ nm and parallel scattering configuration.

(for $x>0$) does indicate a change in optical properties with Sr substitution. Further, the observed broadening of the phonon modes indicates that the scattering is affected by lattice distortions associated with the presence of the large Sr ions and oxygen vacancies corresponding to a more amorphous structure upon introduction of Sr and oxygen vacancies.

However, the substantial decrease in relative scattering intensity between the first- and higher-order excitations of the local breathing mode strongly indicates a direct effect of the Sr doping on the el-ph coupling responsible for the appearance of the FC scattering. We propose that this effect originates from a loss of locality in the interactions through which the FC scattering appears. In stoichiometric $LaFe_{0.5}Cr_{0.5}O_3$ the self-trapping mechanism associated with the photon induced Fe-Cr CT (Ref. 15) produces locally excited $Fe^{4+}O_6$-$Cr^{2+}O_6$ groups which, since all charge carriers are localized to their respective ions, have no quick dissipation channels and are thus effectively decoupled from the rest of the structure. Such a localized system resembles a simple "particle in a box" where the available high-energy excitations are the higher harmonics represented by the higher-order modes seen in the inelastic-scattering response.

As Sr is introduced into $La_{1-y}Sr_yFe_{0.5}Cr_{0.5}O_{3-\delta}$ the compound can retain charge neutrality through the introduction of oxygen vacancies. However, the number of oxygen vacancies experimentally observed by neutron diffraction is smaller than the nominal number needed to electronically balance the compound ($\delta_{expt} \approx 0.05$ and 0.23 while $\delta_{nom}=0.08$ and 0.25 for $x=0.16$ and 0.5, respectively). This indicates that a small number of holes are distributed throughout the structure. We propose that these holes locate on the TM ions causing a number of Fe or Cr ions to take $4+d^4$ (for Fe) or d^2 (for Cr) configurations in the electronic ground state. Both of these electronic configurations are characterized by anisotropic d orbitals and will deform the surrounding oxygen lattice accordingly. These local structural distortions cause a decoherence of the lattice surrounding the sites where the CTs occur. This structural perturbation increases the overlap between the locally excited $Fe^{4+}(d^4)$-$Cr^{2+}(d^4)$ ion complexes responsible for the FC activation and the rest of the lattice, resulting in a loss of locality and rapid decay of the excited state allowing less time for the FC scattering to appear. The presence of some mixed M^{3+}/M^{4+} valence states is also supported by the change in color mentioned above.

Alternatively, the additional holes could form a continuum of mobile charge carriers in the oxygen lattice. This would open up an electronic dissipation channel between the locally excited $Fe^{4+}O_6$-$Cr^{2+}O_6$ groups and the rest of the structure, causing a rapid delocalization of the electronic excitation and a decrease in the lifetime of the FC excitation. Together with the disturbances in the lattice coherence caused by the presence of Sr ions and O vacancies this would also cause a general broadening of the nonresonant phonon modes.

However, four orders of the FC scattering remain for $x=0.16$ (at 80 K, not shown). This indicates that the number of mobile holes in the lattice has to be quite low since they would otherwise quickly eradicate any localized effects. Further, preliminary transport measurements show no metallic behavior in neither $LaFe_{0.5}Cr_{0.5}O_3$ nor $La_{0.5}Sr_{0.5}Fe_{0.5}Cr_{0.5}O_3$.

F. Mode assignment

According to symmetry analysis 24 Raman-active Γ-point modes are allowed in an orthorhombic perovskite belonging to the D_{2h}^{16} space group. Using the *Pnma* setting $7A_g$ and $7B_{2g}$ modes are expected to be active in the crystallographic ac plane under off-resonance conditions.[30,31] (In the *Pbnm* setting these modes have A_g and B_{1g} symmetries.[27]) Of these 14 modes, two involve only A-site ion displacements (one A_g and one B_{2g}) and four are characterized by a combination of A site and oxygen displacements (two A_g and two B_{2g}). Further, there are three oxygen octahedral tilt modes (two A_g and one B_{2g}) and three oxygen bending modes (one A_g and two B_{2g}). Finally, two are oxygen stretching modes, one A_g and one B_{2g}, also referred to as the antisymmetric (AS) and symmetric (SS) stretch modes.[7,21,27] In the ideal *Pnma* structure the B sites are at centers of inversion and no vibrations including B site ions are allowed from symmetry.

The Raman-active vibrational modes in perovskite $AMnO_3$ and $LaCrO_3$ with orthorhombic *Pnma* (*Pbnm*) structure have been extensively studied and a detailed assignment has recently emerged.[18,21–23] Given the structural similarities between these compounds and B site disordered $AFe_{0.5}Cr_{0.5}O_3$ we assume that, apart from the oxygen stretching modes which are intimately linked to the static JT distortion present in $LaMnO_3$,[18] the spectra obtained from these compounds should display qualitative similarities. We also observe that the low-energy spectra obtained from $LaCrO_3$ and $LaFeO_3$ are quite similar (Fig. 12) and propose that the mode assignment for $LaCrO_3$ can be directly transposed onto $LaFeO_3$.

As mentioned earlier it is likely that some amount of local B-site ordering is present in $LaFe_{0.5}Cr_{0.5}O_3$. From this follows that the polarization properties of the nonresonant phonon modes may be influenced by the selection rules of the monoclinic $P2_1/n$ space group. The nature of the Raman-active modes in the monoclinic $P2_1/n$ symmetry and the relation to their *Pnma* counterparts have recently been studied in detail.[32–36] We note in particular that a detailed assignment of the oxygen stretching modes is complicated by the presence of local B-site ordering since the AS and SS modes are active in opposite scattering geometries in *Pnma* and $P2_1/n$ symmetries.[34] In the present measurements the influence of the local ordering is seen by a smearing of the *Pnma* selection rules (Fig. 13). However, despite the presence of this symmetry mixing we perform a preliminary mode assignment based on the *Pnma* setting using the notation established in Ref. 30.

To achieve the present assignment of the nonresonant Γ-point modes in $AFe_{0.5}Cr_{0.5}O_3$ (A=La, Nd, and Gd) the results obtained by Nd and Gd substitution (Fig. 12) as well as from $LaCrO_3$ and $LaFeO_3$ are compared with the polarization-dependent scattering from $LaFe_{0.5}Cr_{0.5}O_3$ (Fig. 13). We initially observe that the Raman-active features in $AFe_{0.5}Cr_{0.5}O_3$, $LaCrO_3$, and $LaFeO_3$ appear in four main groups located below 200 cm^{-1}, between 200 and 350 cm^{-1}, between 400 and 500 cm^{-1} and above 500 cm^{-1} (Figs. 12 and 13) corresponding roughly to the group assignment of modes of A site (A), oxygen tilt (T), oxygen bending (B), and oxygen stretching (S) origin used earlier.

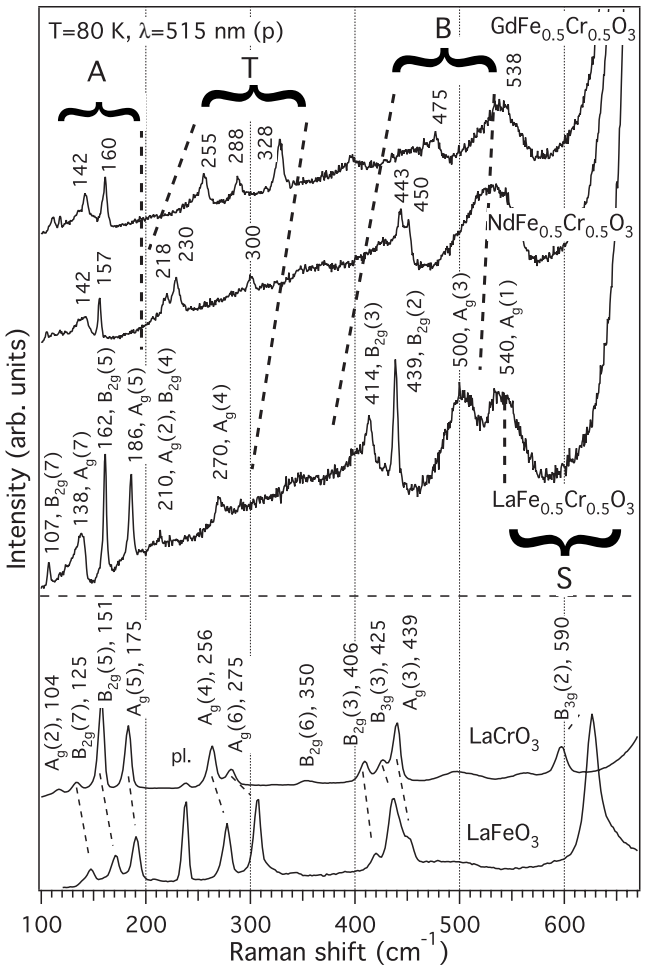

FIG. 12. The low-energy modes in $AFe_{0.5}Cr_{0.5}O_3$ (A=La, Gd, and Nd), $LaCrO_3$ and $LaFeO_3$ at T=80 K, using λ=515 nm and parallel scattering configuration. The proposed mode assignment for $LaFe_{0.5}Cr_{0.5}O_3$ is shown. The given symmetries and frequencies for the modes in $LaCrO_3$ are adopted from Ref. 18. The intensities of the $LaCrO_3$ and $LaFeO_3$ spectra are in fact a lot stronger than those from $AFe_{0.5}Cr_{0.5}O_3$ and have been normalized to enable a convenient comparison between the mode frequencies.

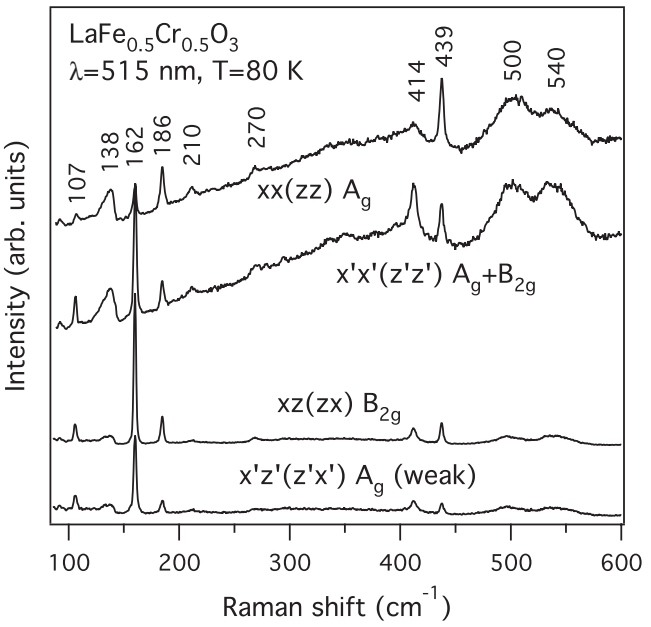

FIG. 13. Polarization dependence and expected mode symmetries of the low-energy Γ-point modes in $LaFe_{0.5}Cr_{0.5}O_3$ at T =80 K using λ=515 nm.

For the oxygen octahedral tilt modes it is firmly established in the literature that the $A_g(4)$ mode is located around 280 cm^{-1} in $LaMnO_3$.[21–23,26,37] Further, this mode shifts to higher energies with isovalent A-site substitution due to an increasing orthorhombic distortion following the decrease in A-site ionic radius.[21–23,26,38] A similar behavior is expected in $AFe_{0.5}Cr_{0.5}O_3$. It has also recently been established that this mode is located at 256 cm^{-1} in $LaCrO_3$,[18] 338 cm^{-1} in $NdMnO_3$, and 370.5 cm^{-1} in $GdMnO_3$.[22] Accordingly we assign the mode at 270 cm^{-1} in $LaFe_{0.5}Cr_{0.5}O_3$ to the $A_g(4)$ tilt mode and propose that this mode shifts to 300 cm^{-1} for A=Nd and 328 cm^{-1} for A=Gd.

Due to the similarity of their normal coordinates it can be expected that the three tilt modes [$A_g(4)$, $B_{2g}(4)$, and $A_g(2)$] should occur at reasonably similar energies, have similar peak profiles and be subject to similar upshifts with A-site substitution.[22,23] In line with this assumption we propose that the weak peak at 210 cm^{-1} in $LaFe_{0.5}Cr_{0.5}O_3$ is caused by the overlapping $B_{2g}(4)$ and $A_g(2)$ modes which split into two distinguishable peaks at 218 and 230 cm^{-1} in $NdFe_{0.5}Cr_{0.5}O_3$ and 255 and 288 cm^{-1} in $GdFe_{0.5}Cr_{0.5}O_3$ (Fig. 12) but the relative assignment of these two modes cannot be firmly established from the present data. We observe, however, that the $A_g(2)$ mode is assign to a peak at 104 cm^{-1} in $LaCrO_3$. Thus, an alternative assignment of the $B_{2g}(4)$ to the 210 cm^{-1} peak and the $A_g(2)$ to either the 107, 138, 162, or 186 cm^{-1} peak (Fig. 12) should perhaps not be completely ruled out for $LaFe_{0.5}Cr_{0.5}O_3$.

In earlier studies of similar compounds the peaks below 200 cm^{-1} are primarily assigned to modes associated with pure A-site vibrations or a combination of A-site and oxygen motion (A-O modes).[18,21–23,38] In particular, the $B_{2g}(5)$ and $A_g(5)$ modes are reported, respectively, at 151 and 175 cm^{-1} in $LaCrO_3$ (Ref. 18) and at 170 and 198 cm^{-1} in $LaMnO_3$.[38] In the present study the 162 cm^{-1} peak in $LaFe_{0.5}Cr_{0.5}O_3$ shows B_{2g}-like selection rules (Fig. 13). Thus, we assign this peak to the $B_{2g}(5)$ mode and the peak at 186 cm^{-1} to the $A_g(5)$ mode. Exchanging La for Nd the $B_{2g}(5)$ and $A_g(5)$ modes show a downshift to 142 and 157 cm^{-1}, respectively, in $NdFe_{0.5}Cr_{0.5}O_3$ probably caused by the increase in ionic mass between La and Nd (Fig. 12). Unexpectedly no similar downshift is seen for $GdFe_{0.5}Cr_{0.5}O_3$ where the corresponding modes are observed at 142 and 160 cm^{-1} (Fig. 12). A similar behavior has been seen in $AMnO_3$ (Refs. 21 and 26) where the low-energy modes are stationary for A-site ions heavier than Nd. A possible explanation for this could be that the downshift due to increasing ionic mass is counteracted by increasing stress in the material structure due to structural distortions. Finally, we propose that the peaks at 107 and 138 cm^{-1} (Figs. 12 and 13) may be assigned to the $B_{2g}(7)$ and $A_g(7)$ A-O modes, respectively. These modes have been reported at similar energies in $LaMnO_3$ (Ref. 38) and $LaCrO_3$.[18] We also note that weak features seen between the characteristic T and B energy regions may be related to the

final two A-O modes [$A_g(6)$ and $B_{2g}(6)$] in line with observations in $LaCrO_3$ (Fig. 12 and Ref. 18).

Above about 400 cm^{-1} we expect modes associated with oxygen bending and stretching vibrations. Of these modes it is well established that the bending vibrations shift to higher energies with A-site substitution in a similar way as the tilt modes.[21–23] On the contrary, the oxygen stretching modes are stationary with A-site substitution resulting in a, by now, well-documented crossing of the $B_{2g}(3)$ bending and the $A_g(1)$ stretching modes in $AMnO_3$.[21–23,26]

Based on these established results and our presented observations (Figs. 12 and 13) we propose for $LaFe_{0.5}Cr_{0.5}O_3$ that the 414 cm^{-1} peak should be assigned to the $B_{2g}(3)$ bending mode. This assignment is supported by the observed polarization dependence of this mode (Fig. 13). Further the 540 cm^{-1} peak is assigned to the $A_g(1)$ AS mode and the 439 and 500 cm^{-1} peaks to the $B_{2g}(2)$ and $A_g(3)$ modes, respectively. With A-site substitution we observe the expected shift to higher energies of the bending modes while the $A_g(1)$ AS mode is stationary (Fig. 12). This behavior results in a merger of the $A_g(3)$ bending mode and the $A_g(1)$ AS mode at 538 cm^{-1} in $GdFe_{0.5}Cr_{0.5}O_3$ (Fig. 12). We note that the $B_{2g}(1)$ SS mode is not observed in these measurements. In the absence of a static JT distortion, the AS and SS modes are expected to be a lot less dominant than in $LaMnO_3$ and are in fact not clearly observed in $LaCrO_3$.[18] Thus, the SS mode may well be hidden beneath the resonantly enhanced local breathing mode.

Temperature-dependent measurements between 300 and 20 K were also performed on $LaFe_{0.5}Cr_{0.5}O_3$ and we briefly mention that the nonresonant Raman-active modes below 600 cm^{-1} increase in height and definition with decreasing temperature. A continuous hardening of the phonons with decreasing temperature is also seen in accordance with a general contraction of the lattice.[24] The phonon mode intensities at the antiferromagnetic (AFM) ordering temperature (T_N=265 K) (Ref. 24) are too low to confirm or discard the presence of spin-lattice interactions similar to those recently observed in some $AMnO_3$ compounds.[23] However, we note that no anomalous softening of the breathing mode is seen similar to that observed in $LaNiMnO_6$.[33]

Leaving the mode assignment of the Γ-point phonons we return to the fact that the scattering above the first-order phonon region is dominated by the higher order FC scattering of the local oxygen breathing mode. A closer inspection of the higher-order scattering shows that each higher order FC mode is flanked by sidebands appearing periodically at lower energies (Fig. 14).

These sidebands appear together with the FC scattering at all temperatures below 300 K and some are present up to seventh order at 80 K using λ=515 nm.[15] An assignment of the main sidebands can be achieved using multiples and combinations of the modes at 500 and 540 cm^{-1} and the FC enhanced local breathing mode. In Fig. 14 we label these modes as A, B, and C, respectively, and propose combinations which reproduce the observed higher-order sideband spectrum.

However, we mention that other mechanisms than multiple phonon and combination scattering of Γ-point phonons may contribute to the sideband formation in the higher-order scattering. Structures similar to those reported here could also originate from higher-order infrared-active longitudinal optical phonons[19,20] or phonon density of states (phDOS) scattering.[39,40] In $LaFe_{0.5}Cr_{0.5}O_3$ several broad background features appear to underlie the Γ-point phonon modes in the 250 to 425, 475 to 575, and 625 to 850 cm^{-1} regions, in particular at low temperatures (Fig. 14). This background profile has similarities with the phDOS scattering seen in $LaMnO_3$.[41]

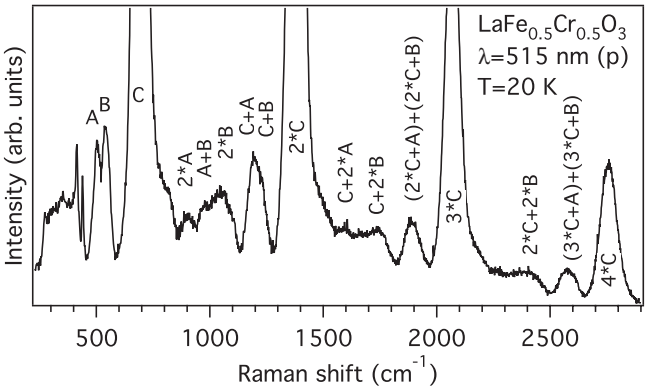

FIG. 14. First four orders of the FC scattering of the breathing mode in $LaFe_{0.5}Cr_{0.5}O_3$ (C, 2^*C, 3^*C, and 4^*C) and the combinations of the oxygen stretching vibrations A, B, and C proposed to produce the higher-order sidebands.

IV. CONCLUSIONS

In this study we have extensively characterized the dominant features of the Raman-active scattering from a large number of Fe-Cr based perovskites with focus on the interaction between the electronic and structural degrees of freedom as seen by the activation of higher-order excitations.

We have studied the emergence of strong electron-lattice interactions in the mixed B-site perovskite solid solution $LaFe_{1-x}Cr_xO_3$ using Raman scattering with λ=515 nm ($\hbar\omega$ =2.41 eV). Our results show that scattering characteristic of a strong electron-phonon interaction is present for $0.02 \leq x \leq 0.98$ indicating that the activation of the Franck-Condon multiphonon scattering is critically sensitive to the presence of both Fe and Cr on the B site and stressing the local nature of this effect. Further, the strong el-ph coupling in $LaFe_{0.5}Cr_{0.5}O_3$ is shown to be sensitive to disturbances in the local coherence of the electronic and structural lattice. This is seen by the rapid decrease in the FC scattering of the local oxygen breathing mode when La is partly replaced by Sr. On the contrary, isovalent A-site substitution (A=La, Nd, and Gd) does not cause a qualitative change of the FC scattering despite the increase in orthorhombic distortion associated with decreasing A-site ionic radii. This indicates that the global structural properties have a limited impact on the appearance of strong el-ph coupling. These results all support the previously proposed Fe to Cr charge-transfer model[15] with the multiphonon scattering appearing according to the Franck-Condon picture.

In addition, we propose that the strong second-order modes present in $LaFeO_3$ are activated by IR LO two-

phonon scattering. The pure oxygen vibrational origin of these two characteristic higher-order scattering profiles is verified using ^{18}O isotope substitution. We also show that the FC multiphonon and IR LO two-phonon scattering mix in $LaFe_{0.96}Cr_{0.04}O_3$ and present a complete assignment of the complex second-order spectrum in this compound. We note a remarkable similarity between spectra obtained from $LaFe_{0.96}Cr_{0.04}O_3$ using $\lambda=515$ nm ($\hbar\omega=2.41$ eV) and $LaFe_{0.5}Cr_{0.5}O_3$ using $\lambda=334$ nm ($\hbar\omega=3.71$ eV) and propose that a simultaneous FC multiphonon and IR LO two-phonon scattering can be activated either by resonance mixing or chemical tuning.

We also observe that the FC multiphonon scattering is not present at room temperature in $LaCrO_3$ and verify recently published results for the low-energy Γ-point phonon modes for this compound, including the structural phase transition at 530 K.[18] Further, we present evidence that the broad peak present in $LaCrO_3$ at 718 cm^{-1} originates from the same local oxygen breathing mode that is resonantly enhanced in the mixed Fe-Cr compounds.

A tentative mode assignment is made for the A_g and B_{2g} modes (*Pnma* setting) in $AFe_{0.5}Cr_{0.5}O_3$ (A=La, Nd, and Gd) and $LaFeO_3$. Vibrations characterized by pure A-site ion displacements are assigned to modes below 200 cm^{-1}, oxygen octahedral tilt vibrations to modes around 270 cm^{-1}, oxygen octahedral bending vibrations to modes around 430 cm^{-1}, and oxygen stretching vibrations to modes above 500 cm^{-1}. The modes assigned to oxygen octahedral tilt, and bending vibrations display large shifts to higher energies with Nd and Gd substitution. This is associated with the interaction between the normal coordinates of these modes and the increase in orthorhombic distortion caused by the smaller ionic radii of Nd and Gd compared to La.

Finally the sidebands which occur close to the higher-order FC modes in $LaFe_{0.5}Cr_{0.5}O_3$ are assigned to combination and multiphonon scattering of specific first-order Raman-active vibrational modes. However, we note that other mechanism such as phonon DOS and IR LO phonon activation may contribute to the observed sideband scattering.

ACKNOWLEDGMENTS

The support of the Swedish Research Council and the Foundation for Strategic Research (Complex Oxide program) is gratefully acknowledged. Work at Houston is supported by the State of Texas through the Texas Center for Superconductivity. We are thankful to B. Schulz for assistance in the UV Raman laboratory and I. Panas for helpful discussions.

*Present address: Department of Cell and Molecular Biology, Uppsala University, Uppsala, Sweden.

[1] A. J. Millis, B. I. Shraiman, and R. Mueller, Phys. Rev. Lett. **77**, 175 (1996).
[2] A. J. Millis, Nature (London) **392**, 147 (1998).
[3] N. A. Babushkina, L. M. Belova, O. Yu. Gorbenko, A. R. Kaul, A. A. Bosak, V. I. Ozhogin, and K. I. Kugel, Nature (London) **391**, 159 (1998).
[4] P. B. Allen and V. Perebeinos, Phys. Rev. Lett. **83**, 4828 (1999).
[5] V. Perebeinos and P. B. Allen, Phys. Rev. B **64**, 085118 (2001).
[6] R. Krüger, B. Schulz, S. Naler, R. Rauer, D. Budelmann, J. Bäckström, K. H. Kim, S.-W. Cheong, V. Perebeinos, and M. Rübhausen, Phys. Rev. Lett. **92**, 097203 (2004).
[7] L. Martín-Carrón and A. de Andrés, Phys. Rev. Lett. **92**, 175501 (2004).
[8] E. Saitoh, S. Okamoto, K. T. Takahashi, K. Tobe, K. Yamamoto, T. Kimura, S. Ishihara, S. Maekawa, and Y. Tokura, Nature (London) **410**, 180 (2001).
[9] D. Polli, M. Rini, S. Wall, R. W. Schoenlein, Y. Tomioka, Y. Tokura, G. Cerullo, and A. Cavalleri, Nature Mater. **6**, 643 (2007).
[10] J. van den Brink, Phys. Rev. Lett. **87**, 217202 (2001).
[11] J. Laverdière, S. Jandl, A. A. Mukhin, and V. Yu. Ivanov, Eur. Phys. J. B **54**, 67 (2006).
[12] K.-Y. Choi, P. Lemmens, G. Güntherodt, Yu. G. Pashkevich, V. P. Gnezdilov, P. Reutler, L. Pinsard-Gaudart, B. Büchner, and A. Revcolevschi, Phys. Rev. B **72**, 024301 (2005).
[13] M. Grüninger, R. Rückamp, M. Windt, P. Reutler, C. Zobel, T. Lorenz, A. Freimuth, and A. Revcolevschi, Nature (London) **418**, 39 (2002).
[14] M. N. Iliev, V. G. Hadjiev, A. P. Litvinchuk, F. Yen, Y.-Q. Wang, Y. Y. Sun, S. Jandl, J. Laverdiére, V. N. Popov, and M. M. Gospodinov, Phys. Rev. B **75**, 064303 (2007).
[15] J. Andreasson, J. Holmlund, C. S. Knee, M. Käll, L. Börjesson, S. Naler, J. Bäckström, M. Rübhausen, A. K. Azad, and Sten-G. Eriksson, Phys. Rev. B **75**, 104302 (2007).
[16] K. Miura and K. Terakura, Phys. Rev. B **63**, 104402 (2001).
[17] A. Dubroka, J. Humlíček, M. V. Abrashev, Z. V. Popović, F. Sapina, and A. Cantarero, Phys. Rev. B **73**, 224401 (2006).
[18] M. N. Iliev, A. P. Litvinchuk, V. G. Hadjiev, Y. Q. Wang, J. Cmaidalka, R.-L. Meng, Y. Y. Sun, N. Kolev, and M. V. Abrashev, Phys. Rev. B **74**, 214301 (2006).
[19] M. V. Abrashev, A. P. Litvinchuk, C. Thomsen, and V. N. Popov, Phys. Rev. B **55**, R8638 (1997).
[20] M. Reedyk, C. Thomsen, M. Cardona, J. S. Xue, and J. E. Greedan, Phys. Rev. B **50**, 13762 (1994).
[21] L. Martín-Carrón, A. de Andrés, M. J. Martínez-Lope, M. T. Casais, and J. A. Alonso, Phys. Rev. B **66**, 174303 (2002).
[22] M. N. Iliev, M. V. Abrashev, J. Laverdière, S. Jandl, M. M. Gospodinov, Y.-Q. Wang, and Y.-Y. Sun, Phys. Rev. B **73**, 064302 (2006).
[23] J. Laverdière, S. Jandl, A. A. Mukhin, V. Yu. Ivanov, V. G. Ivanov, and M. N. Iliev, Phys. Rev. B **73**, 214301 (2006).
[24] A. K. Azad, A. Mellergård, S.-G. Eriksson, S. A. Ivanov, S. M. Yunus, F. Lindberg, G. Svensson, and R. Mathieu, Mater. Res. Bull. **40**, 1633 (2005).
[25] B. Schulz, J. Bäckström, D. Budelmann, R. Maeser, M. Rübhausen, M. V. Klein, E. Schoeffel, A. Mihill, and S. Yoon, Rev. Sci. Instrum. **76**, 073107 (2005).
[26] L. Martín-Carrón, A. de Andrés, M. J. Martínez-Lope, M. T.

Casais, and J. A. Alonso, J. Alloys Compd. **323-324**, 494 (2001).
[27] L. Martín-Carrón and A. de Andrés, Eur. Phys. J. B **22**, 11 (2001).
[28] N. E. Massa, H. Falcón, H. Salva, and R. E. Carbonio, Phys. Rev. B **56**, 10178 (1997).
[29] J. Holmlund, J. Andreasson, C. S. Knee, J. Bäckström, M. Käll, M. Osada, T. Noji, Y. Koike, M. Kakihana, and L. Börjesson, Phys. Rev. B **74**, 134502 (2006).
[30] M. V. Abrashev, J. Bäckström, L. Börjesson, V. N. Popov, R. A. Chakalov, N. Kolev, R.-L. Meng, and M. N. Iliev, Phys. Rev. B **65**, 184301 (2002).
[31] Ph. Daniel, M. Rousseau, A. Desert, A. Ratuszna, and F. Ganot, Phys. Rev. B **51**, 12337 (1995).
[32] C. L. Bull and P. F. McMillan, J. Solid State Chem. **177**, 2323 (2004).
[33] M. N. Iliev, H. Guo, and A. Gupta, Appl. Phys. Lett. **90**, 151914 (2007).
[34] M. N. Iliev, P. Padhan, and A. Gupta, Phys. Rev. B **77**, 172303 (2008).
[35] M. N. Iliev, M. V. Abrashev, A. P. Litvinchuk, V. G. Hadjiev, H. Guo, and A. Gupta, Phys. Rev. B **75**, 104118 (2007).
[36] H. Z. Guo, J. Burgess, E. Ada, S. Street, A. Gupta, M. N. Iliev, A. J. Kellock, C. Magen, M. Varela, and S. J. Pennycook, Phys. Rev. B **77**, 174423 (2008).
[37] M. N. Iliev and M. V. Abrashev, J. Raman Spectrosc. **32**, 805 (2001).
[38] M. N. Iliev, M. V. Abrashev, H.-G. Lee, V. N. Popov, Y. Y. Sun, C. Thomsen, R. L. Meng, and C. W. Chu, Phys. Rev. B **57**, 2872 (1998).
[39] T. P. Martin, Phys. Rev. B **13**, 3617 (1976).
[40] T. P. Martin and S. Onari, Phys. Rev. B **15**, 1093 (1977).
[41] M. N. Iliev, M. V. Abrashev, V. N. Popov, and V. G. Hadjiev, Phys. Rev. B **67**, 212301 (2003).